Supplementary Information

S1. Theoretical Simulations Parameters

Three-dimensional mesh models of the piezoelectric vibrator and the proposed micropump, as well as two-dimensional mesh models of the rectification elements, were constructed in COMSOL Multiphysics 6.0, as shown in Fig. S1. The three-dimensional models employed free quadrilateral meshes, while the two-dimensional models used free triangular meshes. Mesh calibration for fluid dynamics was applied in the fluid flow domains.

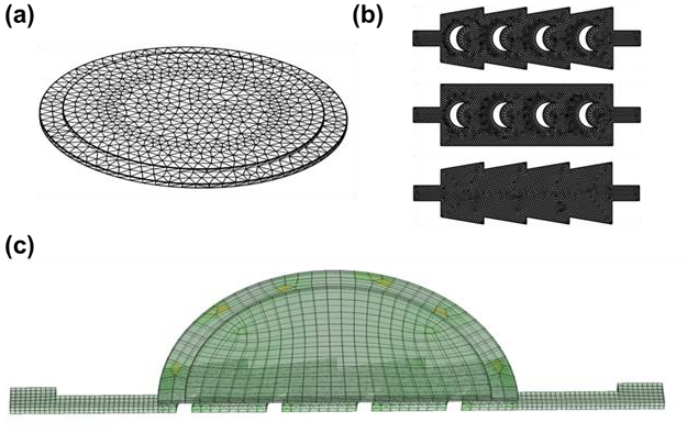

Fig.S1 Simulation grid models. (a) Piezoelectric vibrator. (b) Three types of rectification structures: the series rectification structure, crescent bluff body, and nozzle-diffuser. (c) Overall structure of the valveless. piezoelectric micropump.

Table 1 Material properties of the piezoelectric valveless micropump simulation model

Material	Parameter(unit)	Value
PZT-5H	Coupling matrix (C m^{-2})	$\begin{bmatrix} 0 & 0 & -6.62 \\ 0 & 0 & -6.62 \\ 0 & 0 & 23.24 \\ 0 & 17.03 & 0 \\ 17.03 & 0 & 0 \\ 0 & 0 & 0 \end{bmatrix}$
	Density (kg m^{-3})	7500
	Young's modulus (GPa)	120
Brass	Poisson ratio	0.34
	Density (kg m^{-3})	8960
	Young's modulus (MPa)	0.8
PDMS	Poisson ratio	0.49
	Density (kg m^{-3})	965
Water	Density (kg m^{-3})	998

In the material definition, lead zirconate titanate (PZT-5H) was selected as the piezoelectric ceramic for the piezoelectric vibrator, while brass was used as the metallic substrate of the vibrator. The pump membrane was fabricated from polydimethylsiloxane (PDMS), and water was used as the working fluid. The material properties and structural parameters of the proposed valveless piezoelectric micropump simulation model are summarized in Tables S1 and S2.

Table 2 Parameters and variables of micropump simulation model

Structural unit	Parameter(unit)	Value
PZT	Diameter(mm)	6
	Thickness(mm)	0.1
Substrate	Diameter(mm)	8
	Thickness(mm)	0.1
Upper pump chamber	Diameter(mm)	8
	Depth(μm)	100
Pump membrane	thickness(μm)	100
Bluff body	Spacing (μm)	100-600
	Radius (μm)	300-700
	Side length (μm)	100-600
Nozzle/diffuser	Width (μm)	1600
	Angle (°)	20

In the present simulations, water was modeled as an incompressible Newtonian fluid, and the fluid motion was solved using a transient laminar flow model under the low-Reynolds-number operating conditions of the device. Therefore, the vortices discussed in the manuscript should be understood as local recirculation regions and transient separated flow structures arising from the device geometry, rather than eddies associated with turbulent flow. Since these local flow features mainly occur near the crescent bluff body and the nozzle/diffuser junctions, local mesh refinement was applied in these critical regions to better resolve the velocity gradients, flow turning, and separation behavior. No-slip boundary conditions were imposed on all solid walls, and the fluid domain was solved together with the piezoelectric vibrator and structural deformation using a fully coupled transient electro-solid-liquid model. Under this framework, the simulations were primarily intended to reveal the rectification mechanism of the nested structure and to compare the relative effects of different geometric parameters on flow resistance asymmetry, internal flow field evolution, and net pumping performance.

S2 Micropump preparation and experimental testing

Figure S2 shows photographs of the bottom pump chambers with three different rectification structures, including the crescent bluff body structure, the nested rectification structure, and the nozzle/diffuser structure, together with the dimensional characterization of the assembled micropump.

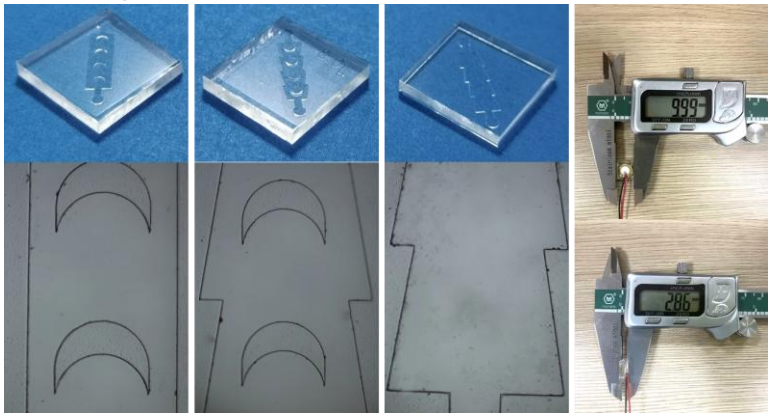

Fig. S2 The bottom pump body of PDMS and the assembled piezoelectric valveless micropump.

An experimental setup was established to evaluate the flow performance of the micropump under different pressure differences, as shown in Fig. S3. The setup mainly consisted of a pressure pump, a buffer reservoir, the micropump, a flowmeter, and a beaker. The pressure pump supplied a constant preset pressure, which was stably transmitted to either the inlet or outlet of the micropump through the buffer reservoir. The flow rate at the opposite end of the micropump was measured in real time by the flowmeter, and the discharged liquid was finally collected in the beaker. This setup was used to characterize the flow behavior of the micropump under different forward and reverse pressure conditions.

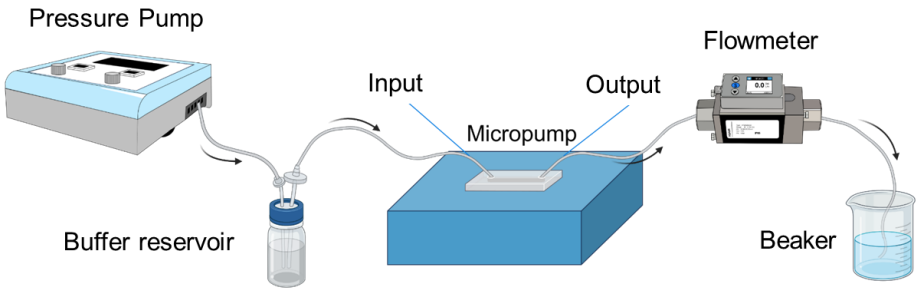

Fig. S3 Flow resistance measuring experiment.

S3. Influence of nested rectification structure height on the flow field

To further illustrate the mechanism underlying the effect of the nested rectification structure height on micropump performance, the simulated internal flow fields for different structure heights are presented in Fig. S4. Figure S4(a)-(f) correspond to nested rectification structure heights of 50, 100, 150, 200, 250, and 300 μm, respectively. As indicated by the velocity color scale and vector distributions, the internal flow velocity gradually increases as the structure height increases from 50 to 200 μm, and reaches its maximum at 200 μm. When the structure height is further increased to 250 and 300 μm, the flow velocity decreases significantly.

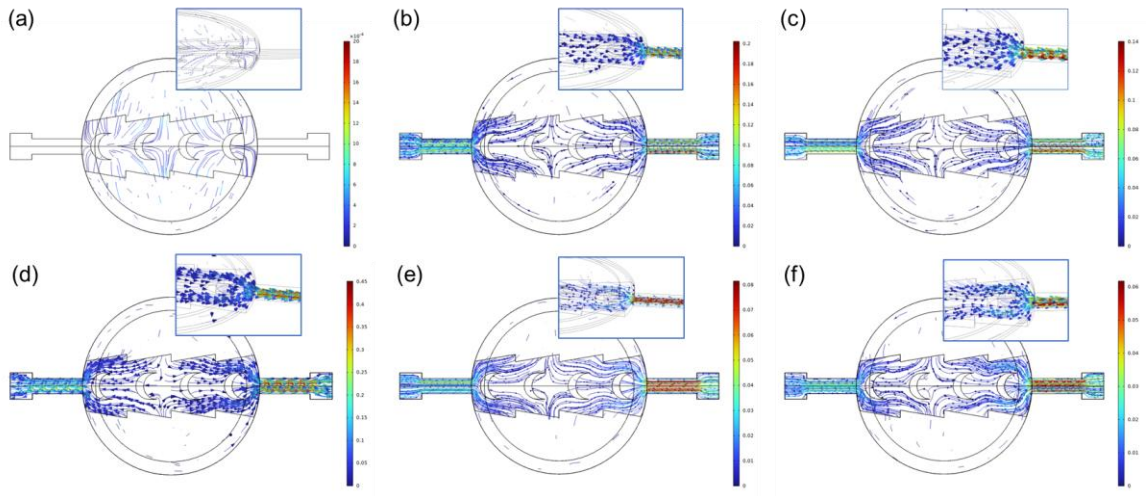

Fig. S4 Simulated internal flow fields of the micropump with different heights of the nested rectification structure: (a) 50 μm, (b) 100 μm, (c) 150 μm, (d) 200 μm, (e) 250 μm, and (f) 300 μm. The insets show enlarged views of the local flow field near the nested rectification region.

This trend is consistent with the net flow rate shown in Fig. 5(h). When the nested rectification structure is too low, the flow passage is overly restricted, which increases viscous dissipation and suppresses effective fluid transport. In contrast, when the structure height becomes excessively large,

the spatial confinement and directional guiding effects of the bluff body and nozzle/diffuser are weakened, resulting in reduced rectification efficiency.

S4. Experimental effect of driving frequency on the net flow rate of the micropump

At a fixed driving voltage of 30 V, the net flow rate of the micropump was experimentally measured over the frequency range of 50-500 Hz, as shown in Fig. S5. The net flow rate first increased with increasing driving frequency, reached a maximum at 200 Hz, and then decreased as the frequency was further increased. This result is consistent with the frequency-selection rationale discussed in the main text. In Section 3.1, the vibration analysis and amplitude characterization of the piezoelectric vibrator provide guidance for selecting an appropriate low-frequency operating range. Based on this frequency range, the flow rate measurements shown in Fig. S5 were further carried out to evaluate the pumping performance experimentally. At relatively low frequencies, increasing the driving frequency enhances the number of effective pumping cycles per unit time and thus increases the net flow rate. However, when the driving frequency becomes too high, the filling and discharge processes cannot fully follow the rapid oscillation of the pump chamber, which reduces the effective transported volume per cycle. Therefore, 200 Hz was identified as the optimal operating frequency and was used in the subsequent experiments on the effect of voltage.

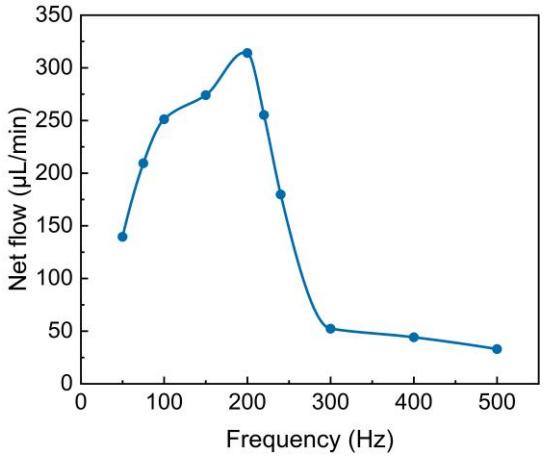

Fig. S5 Experimental effect of frequency on the net flow rate of the micropump at a fixed driving voltage of 30 V.